ACS APPLIED MATERIALS & INTERFACES

Research Article

www.acsami.org

Direct Synthetic Control over the Size, Composition, and Photocatalytic Activity of Octahedral Copper Oxide Materials: Correlation Between Surface Structure and Catalytic Functionality

Michelle A. Nguyen,[†] Nicholas M. Bedford,[‡] Yang Ren,[§] Elsayed M. Zahran,[†] Robert C. Goodin,[∥] Fatima F. Chagani,[†] Leonidas G. Bachas,[†] and Marc R. Knecht*[,†]

[†]Department of Chemistry, University of Miami, 1301 Memorial Drive, Coral Gables, Florida 33146, United States

[‡]Applied Chemicals and Materials Division, National Institute Standards and Technology, 325 Broadway, Boulder, Colorado 80305, United States

[§]X-ray Science Division, Argonne National Laboratory, 9700 S. Cass Avenue, Argonne, Illinois 60439, United States

[∥]Westminster Christian School, 6855 SW 152nd Street, Palmetto Bay, Florida 33157, United States

Supporting Information

ABSTRACT: We report a synthetic approach to form octahedral Cu_2O microcrystals with a tunable edge length and demonstrate their use as catalysts for the photodegradation of aromatic organic compounds. In this particular study, the effects of the Cu^{2+} and reductant concentrations and stoichiometric ratios were carefully examined to identify their roles in controlling the final material composition and size under sustainable reaction conditions. Varying the ratio and concentrations of Cu^{2+} and reductant added during the synthesis determined the final morphology and composition of the structures. Octahedral particles were prepared at selected Cu^{2+}:glucose ratios that demonstrated a range of photocatalytic reactivity. The results indicate that material composition, surface area, and substrate charge effects play important roles in controlling the overall reaction rate. In addition, analysis of the post-reacted materials revealed photocorrosion was inhibited and that surface etching had preferentially occurred at the particle edges during the reaction, suggesting that the reaction predominately occurred at these interfaces. Such results advance the understanding of how size and composition affect the surface interface and catalytic functionality of materials.

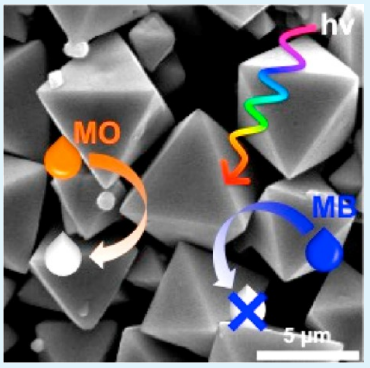

KEYWORDS: *Cu_2O, octahedra, size control, photodegradation, compositional effects*

INTRODUCTION

Because of the impending energy crisis, photocatalytic processes have become particularly attractive, based on their reliance on renewable solar light as the main energy source to drive the reaction. Over the past few decades, major advances have occurred in the design and fabrication of highly active and efficient photocatalysts as viable alternatives to conventional catalytic materials.[1−3] Various photocatalysts, especially metal oxide semiconductors such as TiO_2 and ZnO, have been extensively investigated for their use in photo-based processes.[4−9] Unfortunately, their wide band gaps restrict their light absorption capabilities to ultraviolet wavelengths only. This results in inefficient use of solar energy as most of the solar spectrum is in the visible and infrared regions;[10] photons within this energy range cannot photoexcite TiO_2 and ZnO.[11,12] Alternatively, the use of narrow band gap semiconductor photocatalysts could effectively exploit visible light absorption for photoexcitation and electron/hole pair generation to take advantage of a significantly greater portion of solar energy that is available.

An exciting material for visible light photocatalysis is Cu_2O, which is a *p*-type semiconductor with a small band gap of 2.17 eV.[13] Cu_2O is inexpensive, abundantly available, and has already shown promising activity for solar and energy applications, such as visible light-driven proton reduction for H_2 evolution,[14,15] solar energy photovoltaics,[16] and electrode material in lithium-ion batteries.[17,18] Importantly, Cu_2O has become an attractive material for the photocatalytic degradation of environmental pollutants,[3,19−21] where it has demonstrated the ability to break down aromatic dyes that are known to be difficult to degrade.[22] This reaction typically occurs through the generation of reactive oxygen species at the metal oxide surface, leading to pollutant degradation.[23−25] By controlling the facet display of the Cu_2O via changes in the particle shape and size, the visible-light-based reactivity of the materials could be enhanced.

To understand the reactivity, Cu_2O nanocrystals and microcrystals have been prepared in various morphologies, including cubes,[26] spheres,[27] octahedra,[28] and rhombic dodecahedra.[29] Although various approaches have been followed for the production of shape- and size-controlled

Received: December 30, 2014
Accepted: May 26, 2015
Published: May 26, 2015

DOI: 10.1021/acsami.5b04282
ACS Appl. Mater. Interfaces 2015, 7, 13238−13250

Scheme 1. Procedure for the Fabrication of Cu_2O Octahedra Using Glucose as the Reductant Leading to Particles with Tunable Edge Lengths

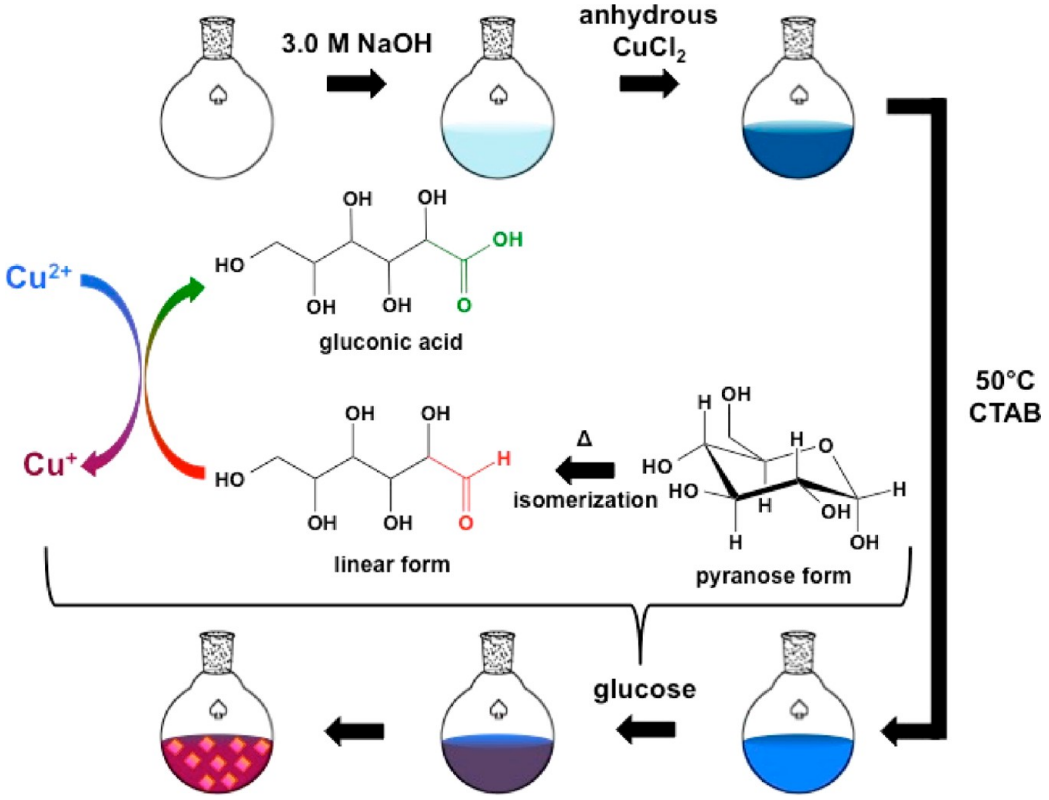

Cu_2O particles, many of these methods are energy-intensive (>100 °C) with long reaction times. As such, the development of sustainable, facile, and low-temperature routes to size- and shape-controlled Cu_2O materials has gained increasing interest, but the ability to control both parameters simultaneously remains challenging. For example, Gou et al. reported the synthesis of Cu_2O nanocubes with a tunable edge length of 25−200 nm by using $CuSO_4$, poly(ethylene) glycol, ascorbic acid, and NaOH in water at room temperature.[26] Zhang and co-workers have reacted $CuCl_2$, NaOH, and sodium ascorbate or hydrazine at room temperature to form Cu_2O nanocubes, octahedrons, cuboctahedrons, spheres, and facet-etched cubes.[30] In an additional approach, Liang et al. synthesized polyhedral 50-facet Cu_2O microcrystals enclosed with high-index {211}, {522}, or {311} facets by mixing $Cu(CH_3COO)_2$ and glucose at 70 °C.[31] Such energy-efficient processes are required for sustainable routes toward important Cu_2O structures; however, the effects of the reagents in the reaction mixture remain unclear. For instance, several reductants are employed to partially reduce Cu^{2+} to Cu^+ in the final Cu_2O materials. The choice of reductant is of critical importance, because it must be strong enough to reduce the metal ions under kinetically controlled conditions and to slowly grow the oxide crystal of a specific shape; such effects will undoubtedly play a role in determining the final particle size. As a result, the identity, concentration, and reaction rate of the reductant are of significant importance to the final structure, where little understanding of such effects is known.

In this study, we present a facile synthetic method to generate Cu_2O octahedral microcrystals, where the edge length of the structure can be selected for based on reductant effects on the reaction. The structures are prepared in aqueous solution using $CuCl_2$, NaOH, cetyltrimethylammonium bromide (CTAB), and glucose at a relatively low temperature (50 °C), which is notably lower than that observed in many other synthetic approaches.[32,33] Glucose was specifically selected as the reductant, because (i) it is an ecologically friendly alternative to standard reductants and (ii) the rate of reduction can be easily controlled, based on glucose isomerization. Such reductant effects play a significant role in controlling the overall material composition, morphology, and dimensions. Once prepared, the materials were extensively characterized to confirm their morphology, size, and composition using scanning electron microscopy (SEM), powder X-ray diffraction (XRD), X-ray photoelectron spectroscopy (XPS), ultraviolet−visible light diffuse reflectance spectroscopy (UV−vis DRS), and Brunauer−Emmett−Teller (BET) analysis. From the synthetic analysis, the effects of the Cu^{2+} and reductant concentrations and stoichiometric ratios were investigated, indicating that the size and composition of the materials were directly related to the Cu^{2+} concentration and rate of reduction. Once the materials were characterized, their photocatalytic activities were investigated by monitoring the degradation of methyl orange and methylene blue. From this study, the effects of the material composition and surface area were observed to play a significant role in the reactivity. Of importance, analysis of the materials after the reaction revealed a substantial change in particle surface structure, where etching at the oxide edges was noted. This suggests that such regions may serve as the photocatalytic active site for radical generation, thus contributing to the understanding of photocatalytic mechanisms and charge carrier pathways. These results are important as they provide a route to size-controlled Cu_2O materials for photocatalysis. They also provide intriguing information

DOI: 10.1021/acsami.5b04282
ACS Appl. Mater. Interfaces 2015, 7, 13238−13250

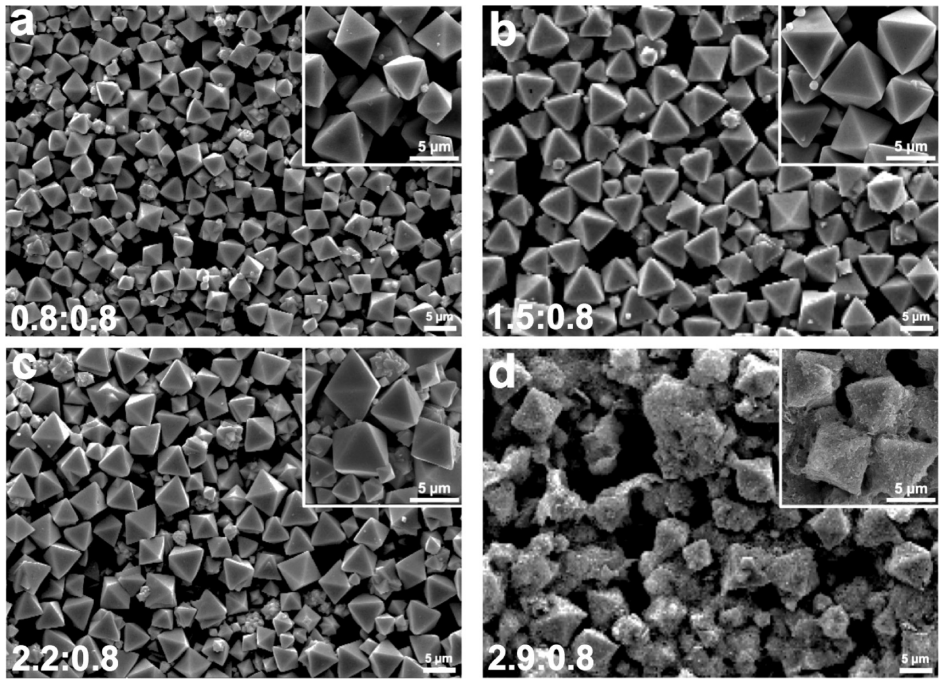

Figure 1. SEM images of the Cu_2O octahedra synthesized in the presence of CTAB at Cu^{2+}:glucose mole ratios of (a) 0.8:0.8, (b) 1.5:0.8, (c) 2.2:0.8, and (d) 2.9:0.8. Scale bars = 5 μm.

concerning the catalytic activity of these structures, based on particle composition and size, including potential surface reaction sites.

MATERIALS AND METHODS

Chemicals. NaOH was acquired from Acros Organics, while anhydrous $CuCl_2$, methyl orange, and methylene blue were attained from Alfa Aesar. CTAB and glucose were purchased from Sigma–Aldrich. All chemicals were used as-received, without further purification. Milli-Q water (18 MΩ·cm) was used for all experiments.

Synthesis of Cu_2O Octahedra. The following synthesis was adapted from a previous study for the fabrication of Cu-based nanotubes.[34] The production of the octahedra is described using the Cu^{2+}:glucose ratio to differentiate the samples. In a round-bottom flask, 0.8, 1.5, 2.2, or 2.9 mmol of anhydrous $CuCl_2$ were dissolved in 100 mL of 3.0 M aqueous NaOH by stirring and sonicating. After placing the flask in a 50 °C oil bath, 6 mmol of CTAB was added directly to the solution, which was then stirred for 30 min at the elevated temperature. Immediately after removing the flask from the oil bath, 0.8 mmol of glucose was added. Afterward, the solution was stirred for 1 h at room temperature. The precipitate was collected by centrifugation, washed several times with water and ethanol, and dried under vacuum for at least 12 h. Separate reactions were also conducted using the exact same procedures; however, the glucose amount was increased to be equal to the Cu^{2+} amounts of 1.5, 2.2, or 2.9 mmol.

Photocatalytic Degradation Experiments. For each photocatalytic experiment, sufficient Cu_2O materials were added to reach either a surface area of 0.065 m^2 (constant-surface area conditions), as determined by BET analysis, or a mass of 10.0 mg (constant-mass conditions). For this, the Cu_2O sample was placed into a 100 mm × 50 mm crystallizing dish, to which 20.0 mL of a 30.0 mg/L (91.6 μM) aqueous methyl orange or methylene blue solution was added. Next, the dish was sonicated for 10 s and then capped with a quartz cover. Before light irradiation, the reactions were stirred for 30 min in darkness to allow for dye adsorption to the particle surface. Once complete, the reaction was stirred while being irradiated with an Oriel Sol1A Class ABB solar simulator employing a 1000 W Xe arc lamp operating at ∼100 mW/cm^2. The sample to light source distance was ∼20 cm. Aliquots (150 μL) of the reaction mixture were extracted every 10 min for 3.0 h to analyze the reaction progression via UV-vis analysis.

Characterization. SEM was performed using an FEI XL-30 Field Emission ESEM/SEM operating at 20 kV. To prepare the sample, the Cu_2O materials were dispersed in ethanol via sonication, after which 10 μL of the sample was drop-casted onto an aluminum stub. High-energy X-ray diffraction (HE-XRD) patterns were collected at the Advanced Photon Source at Argonne National Laboratory, using Beamline 11-ID-C at 115 keV. Powders of Cu_2O microcrystals were loaded into 2 mm outer diameter thin-walled quartz capillaries for each sample. A large area detector was employed to collect two-dimensional (2D) patterns, which were then integrated into one-dimensional (1D) patterns using the Fit2D program.[35] XPS characterization was performed on a Perkin–Elmer Model 5100 XPS system. UV-vis DRS analysis was completed on a Shimadzu Model UV-2600 system. BET surface area analysis was carried out on a Quantachrome Model NOVA 1200 system. Finally, UV-vis spectra of the reaction analysis were acquired using an Agilent Model 8453 UV-vis spectrophotometer employing a 2.00 mm path length quartz cuvette.

RESULTS AND DISCUSSION

Materials Synthesis and Characterization. In this contribution, size-controlled Cu_2O octahedra are generated using a mixture of $CuCl_2$, NaOH, CTAB, and glucose at a relatively low temperature (Scheme 1). For this, glucose acts as the reductant at 50 °C, where it isomerizes to the linear form to expose an aldehyde[36] that can reduce Cu^{2+} to Cu^{+}.[37] As this reduction process is anticipated to lead to control over the morphology and composition of the final structure, fabrication of Cu_2O was processed where the Cu^{2+}:glucose ratio was varied, as was the actual concentrations of the two species. This was performed to determine the effects of glucose over the final morphology of the materials, where minimal understanding of the reductant control over particle size, structure, and composition is presently known.

In the initial reaction system, the Cu^{2+} concentration was gradually increased, while the glucose and CTAB concentrations remained constant. In this regard, the materials were

DOI: 10.1021/acsami.5b04282
ACS Appl. Mater. Interfaces 2015, 7, 13238–13250

Table 1. Structural and Photocatalytic Degradation of Methyl Orange Reactivity Comparison for the Cu_2O Octahedra

Cu^{2+}:glucose mole ratio	edge length (μm)	surface Cu^+ percentage	E_g (eV)	surface area[a] (m^2/g)	k_{mass} ($\times 10^{-2}$ min^{-1})	k_{SA} ($\times 10^{-2}$ min^{-1})
0.8:0.8	2.7 ± 0.8	80.8%	2.03	0.69	1.18 ± 0.05	5.16 ± 0.66
1.5:0.8	4.4 ± 1.1	64.0%	2.02	0.82	2.01 ± 0.17	2.80 ± 0.57
2.2:0.8	1.7 ± 0.6	46.4%	2.00	3.05	0.69 ± 0.07	0.05 ± 0.02
	4.4 ± 1.1					
2.9:0.8	4.5 ± 0.8	38.0%	1.98	12.93	0.70 ± 0.05	0.08 ± 0.07
1.5:1.5	2.4 ± 0.5	61.4%	2.02	0.43	1.31 ± 0.53	2.87 ± 0.27
2.2:2.2	3.6 ± 0.7	71.6%	2.02	0.56	0.51 ± 0.12	4.18 ± 1.42
2.9:2.9	4.3 ± 1.0	61.9%	2.03	0.24	0.30 ± 0.09	2.75 ± 0.79

[a]Surface area determined via BET.

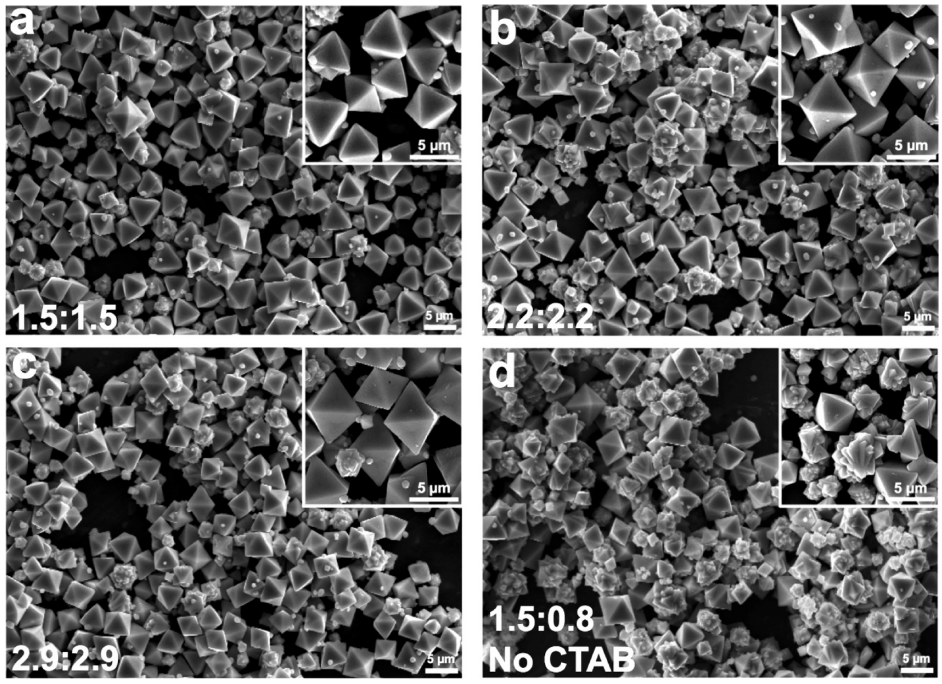

Figure 2. SEM images of the Cu_2O octahedra fabricated in the presence of CTAB with Cu^{2+}:glucose molar ratios of (a) 1.5:1.5, (b) 2.2:2.2, and (c) 2.9:2.9. Panel d presents the materials prepared at a Cu^{2+}:glucose mole ratio of 1.5:0.8, but in the absence of CTAB. Scale bars = 5 μm.

synthesized with Cu^{2+}:glucose ratios of 0.8:0.8, 1.5:0.8, 2.2:0.8, and 2.9:0.8. Note that the values listed in the ratios represent the actual number of millimoles of the reagent in the reaction, and this notation will be employed herein to differentiate samples. Upon completion, a brick-red precipitate was generated for most of the samples, consistent with previous strategies for the production of Cu_2O.[38,39] For the 2.9:0.8 sample, however, a black precipitate was observed, indicating a change in particle composition and/or morphology. Once the materials were purified and dried, they were imaged using SEM. Figure 1 presents the morphology of the particles prepared using the constant glucose concentration. Generally, high yields of well-defined octahedral Cu_2O structures were generated with varying edge lengths based on the Cu^{2+}:glucose ratio. The average edge lengths for each sample are summarized in Table 1. Figure 1a specifically presents the materials fabricated at a Cu^{2+}:glucose ratio of 0.8:0.8. Here, well-defined octahedrally shaped materials are generated with an average edge length of 2.7 ± 0.8 μm. Shape classification analysis, as shown in Table S1 in the Supporting Information, indicated that 79% of the materials were octahedra. As the Cu^{2+}:glucose ratio changed to 1.5:0.8 (Figure 1b), a clear shift in particle size was observed. While it was evident that octahedral materials were again prepared (92% octahedra in the sample), the average particle size increased to 4.4 ± 1.1 μm. Interestingly, for the 2.2:0.8 materials (Figure 1c), a bimodal material set was noted with 78% of the materials being octahedra. For this, two populations were observed, with edge lengths of 1.7 ± 0.6 and 4.4 ± 1.1 μm. Finally, when the highest Cu^{2+} concentration was employed (2.9:0.8, see Figure 1d), the morphology of the materials began to vary. While the structures were generally octahedral (76% were classified as octahedra), the surface became very rough. For these structures, an edge length of 4.5 ± 0.8 μm was determined. For all particle sizing and shape analyses, at least 100 particles were measured over multiple SEM images (see Figure S1 and Table S1 in the Supporting Information).

While interesting materials were prepared using a constant glucose concentration, greater reductant amounts may directly affect the material composition, size, and/or shape. To examine the effect of the reductant, a second set of materials was generated where the Cu^{2+} concentrations employed were the same as those above; however, the glucose concentrations were increased to match the amount of Cu^{2+}. In this system, as the amount of Cu^{2+} increased, the edge length of the structures also linearly increased. Figure 2a specifically presents the materials

DOI: 10.1021/acsami.5b04282
ACS Appl. Mater. Interfaces 2015, 7, 13238−13250

prepared at a Cu^{2+}:glucose ratio of 1.5:1.5. Note that a lower Cu^{2+} and glucose concentration (0.8:0.8) sample was prepared above, which also maintains equal concentrations of Cu^{2+} and glucose. In this sample, Cu_2O octahedra are again prepared (86% octahedra) with an edge length of 2.4 ± 0.5 μm. As the reagent concentrations were increased in the 2.2:2.2 (Figure 2b) and 2.9:2.9 (Figure 2c) samples, the average edge lengths also increased to 3.6 ± 0.7 and 4.3 ± 1.0 μm, respectively. For these structures, only a single population of brick-red materials was noted, where either 75% (2.2:2.2) or 67% (2.9:2.9) of the structures were octahedra.

To understand the effect and fate of the surfactant over the particle morphology, a set of control experiments was conducted. In this initial study, the Cu_2O materials were prepared at a Cu^{2+}:glucose ratio of 1.5:0.8 in the absence of CTAB (Figure 2d). In this reaction, the majority of materials presented multiple interfaces with sharp edges, suggesting overgrowth of octahedra. Occasionally octahedra were present in the sample, but they represented only a minor fraction of the population (24%). Such a population percentage is significantly lower than those achieved for materials fabricated with CTAB present in the reaction mixture. These structures were also polydisperse in size, ranging from 0.8 μm to 6.0 μm in size. This suggested that the surfactant played an important role in controlling the octahedral morphology; however, additional studies were completed to determine the fate of the CTAB. For this, materials fabricated at a ratio of 1.5:0.8 in both the presence and absence of CTAB were also characterized by thermogravimetric analysis (TGA) and IR spectroscopy (see Figure S2 in the Supporting Information). Generally, both characterization methods indicated that no CTAB was retained by the materials after the extensive washing procedure; no mass loss of CTAB combustion was evident from TGA, and no vibrations of the surfactant were observed in the IR analysis. From this, it is evident that the surfactant plays a role in controlling the morphology and particle size. Furthermore, the TGA and IR analyses indicate that the interactions between the surfactant and oxide are likely to be quite weak, as evidenced by the fact that the purification process completely removes this component. Taken together, this suggests that the surfactant is responsible for controlling the particle morphology during the oxide growth process, but this condition is not required to maintain long-term particle shape stability.

To study the phase purity of the materials, XRD was employed (Figure 3). Diffraction patterns of the as-synthesized structures were compared with patterns for bulk Cu_2O and CuO, where every peak can be indexed to either composition. The diffraction patterns for the materials fabricated at a Cu^{2+}:glucose ratio of 0.8:0.8, 1.5:0.8, or 2.2:0.8 are consistent with the cubic phase of Cu_2O, displaying reflections at 2.08, 2.55, 2.95, 4.17, 4.89, and 5.10 $Å^{-1}$, corresponding to the (110), (111), (200), (220), (311), and (222) lattice planes of Cu_2O, respectively.[40] When the highest Cu^{2+} concentration was used to give a Cu^{2+}:glucose ratio of 2.9:0.8, one minor CuO peak was observed at 2.71 $Å^{-1}$, indexed to the (111) lattice.[40] Such results suggest that Cu_2O is the dominant species present in the samples with lower Cu^{2+} concentrations, but that the amount of CuO in the material increases in the 2.9:0.8 structures. In comparison, for the materials generated at equal Cu^{2+} and glucose concentrations (1.5:1.5, 2.2:2.2, and 2.9:2.9 samples), the XRD patterns can be fully ascribed to Cu_2O with no CuO reflections. This indicates that the amount of the reductant in the sample and the reagent concentrations play an important role in controlling particle size and composition; however, additional analysis via XPS was employed to corroborate such effects.

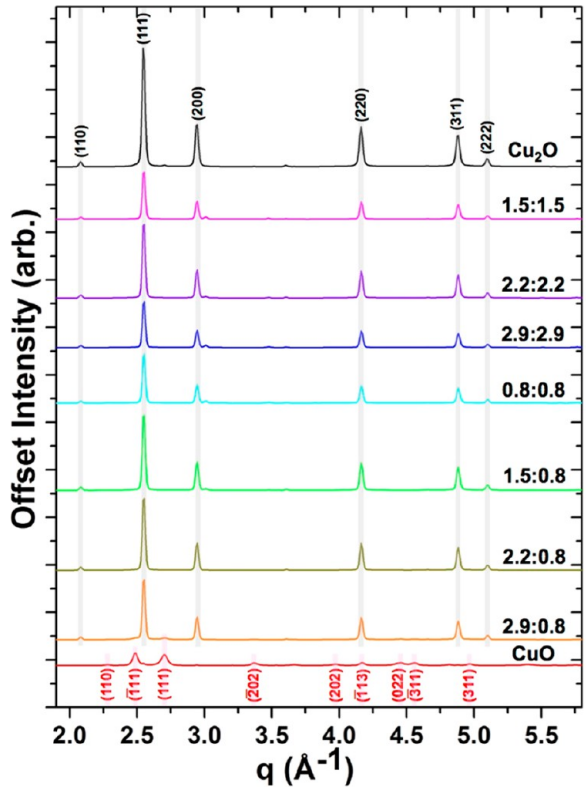

Figure 3. XRD patterns of the octahedral materials. The gray lines denote diffraction peaks attributed to Cu_2O, while the pink lines denote peaks indexed to CuO.

The surface composition of the as-synthesized materials was examined via XPS analysis. Figure 4a presents the analysis for the 0.8:0.8 structures, where peak fitting of the data revealed two Cu $2p_{3/2}$ peaks at 932.5 and 933.7 eV, consistent with Cu^+ and Cu^{2+}, respectively.[41] From this assessment, the materials were composed of 80.8% Cu^+ and 19.2% Cu^{2+}. Note that this analysis is only able to analyze the surface of the octahedra and not the entire material; the amount of oxidized Cu^{2+} is likely to be higher at the surface, because of O_2 exposure. Similar analyses were then conducted for all of the materials prepared at the selected ratios. Generally, higher amounts of Cu^{2+} were observed from those samples with low glucose and high Cu concentrations in the reaction. For instance, when the materials were fabricated at Cu^{2+}:glucose ratios of 1.5:0.8, 2.2:0.8, and 2.9:0.8, the amount of surface Cu^+ in the samples decreased linearly, with values of 64.0%, 46.4%, and 38.0%, respectively, with Cu^{2+} making up the balance of Cu. Note the enhancement of the broad peak at ~942 eV as the Cu^{2+}:glucose ratio increases. This peak arises from the shakeup structure associated with the presence of CuO.[42] When the amount of glucose in the reaction was increased and maintained at the same concentration as that of the Cu^{2+} in the reaction, as in the 1.5:1.5, 2.2:2.2, and 2.9:2.9 samples, the amount of Cu^+ in the sample remained roughly similar, ranging between 61.4% and 71.6%. Figure 4h presents a comparison in the amount of Cu^+ in the sample, indicating that higher amounts of Cu^+ are present in the sample at higher glucose concentrations. While the surface (XPS) and bulk (XRD) measurements corroborate each other to suggest that Cu_2O is present in all samples, XPS

DOI: 10.1021/acsami.5b04282
ACS Appl. Mater. Interfaces 2015, 7, 13238−13250

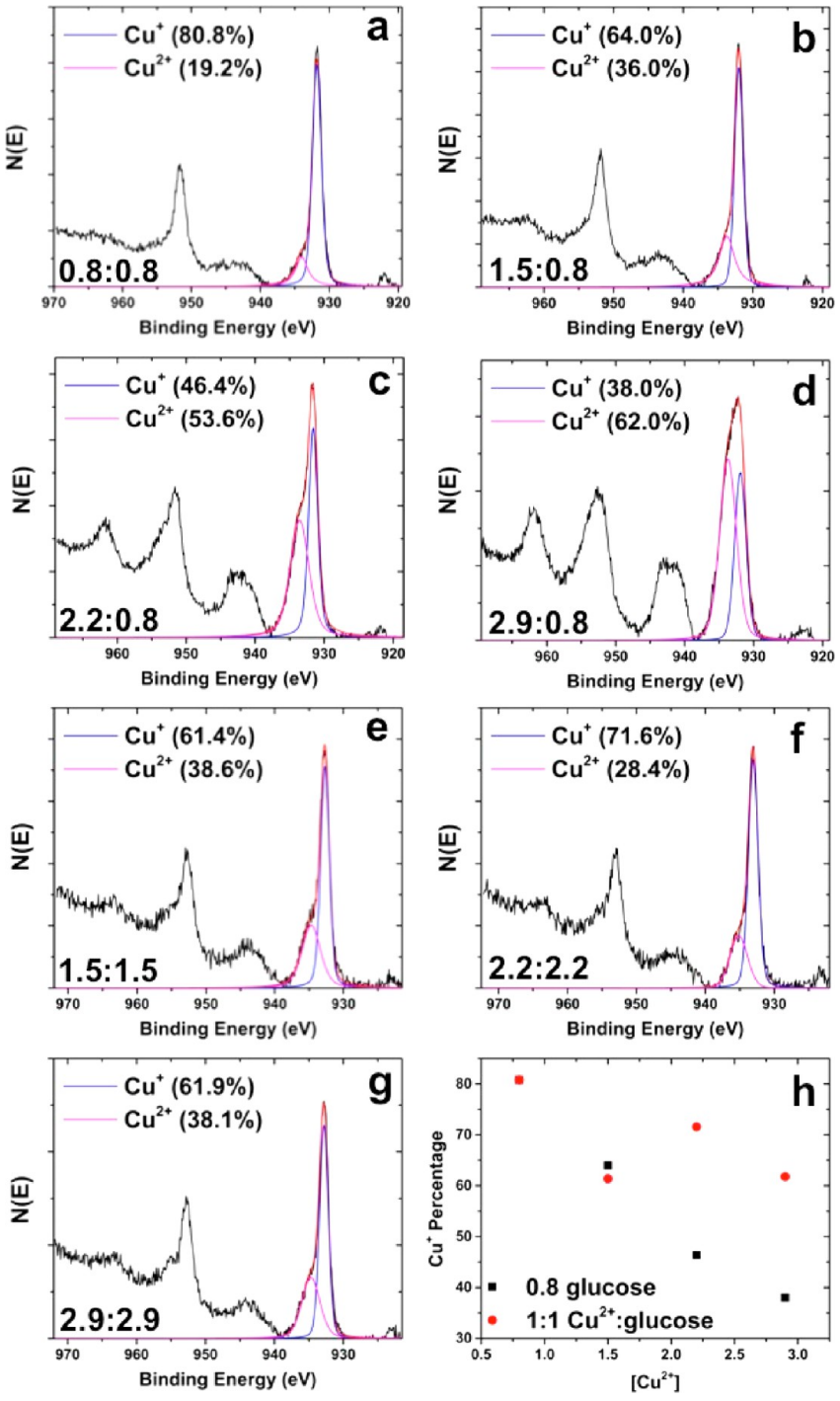

Figure 4. XPS analysis of the Cu_2O octahedral materials prepared at Cu^{2+}:glucose mole ratios of (a) 0.8:0.8, (b) 1.5:0.8, (c) 2.2:0.8, (d) 2.9:0.8, (e) 1.5:1.5, (f) 2.2:2.2, and (g) 2.9:2.9. Panel h shows a comparison of the Cu^+ percentage in the sample as a function of the material.

analysis indicates the presence of surface Cu^{2+} for all the samples. This is attributed to the relatively minor amount, as compared to the total structure as observed via XRD, and amorphous nature of CuO as a result of Cu_2O surface oxidation.[43−45]

The UV-vis absorbance properties of the materials were assessed using UV-vis DRS, and the absorption spectra of the Cu_2O structures are presented in Figure 5a. The particles displayed a strong absorption in the visible region, where the onset of visible light absorption for the 2.9:0.8 sample started at ∼750 nm, compared to ∼650 nm for all of the other Cu_2O octahedra. This suggests that the composition of the 2.9:0.8 sample is different from the other materials. To support this hypothesis, the band gaps of the Cu_2O octahedra were determined by using the Kubelka−Munk function, $F(R_\infty)$, where the values can be obtained from the tangent line of the Tauc plot.[46] As presented in Figure 5b, the band gap of the 0.8:0.8 sample was calculated to be 2.03 eV, which is lower than that of Cu_2O (2.17 eV).[13] This is likely associated with the small amount of CuO in the sample, which is supported by the observed trends in band-gap energies. Generally, the band gaps correlated well with the amount of oxidized Cu^{2+} in the sample,

DOI: 10.1021/acsami.5b04282
ACS Appl. Mater. Interfaces 2015, 7, 13238−13250

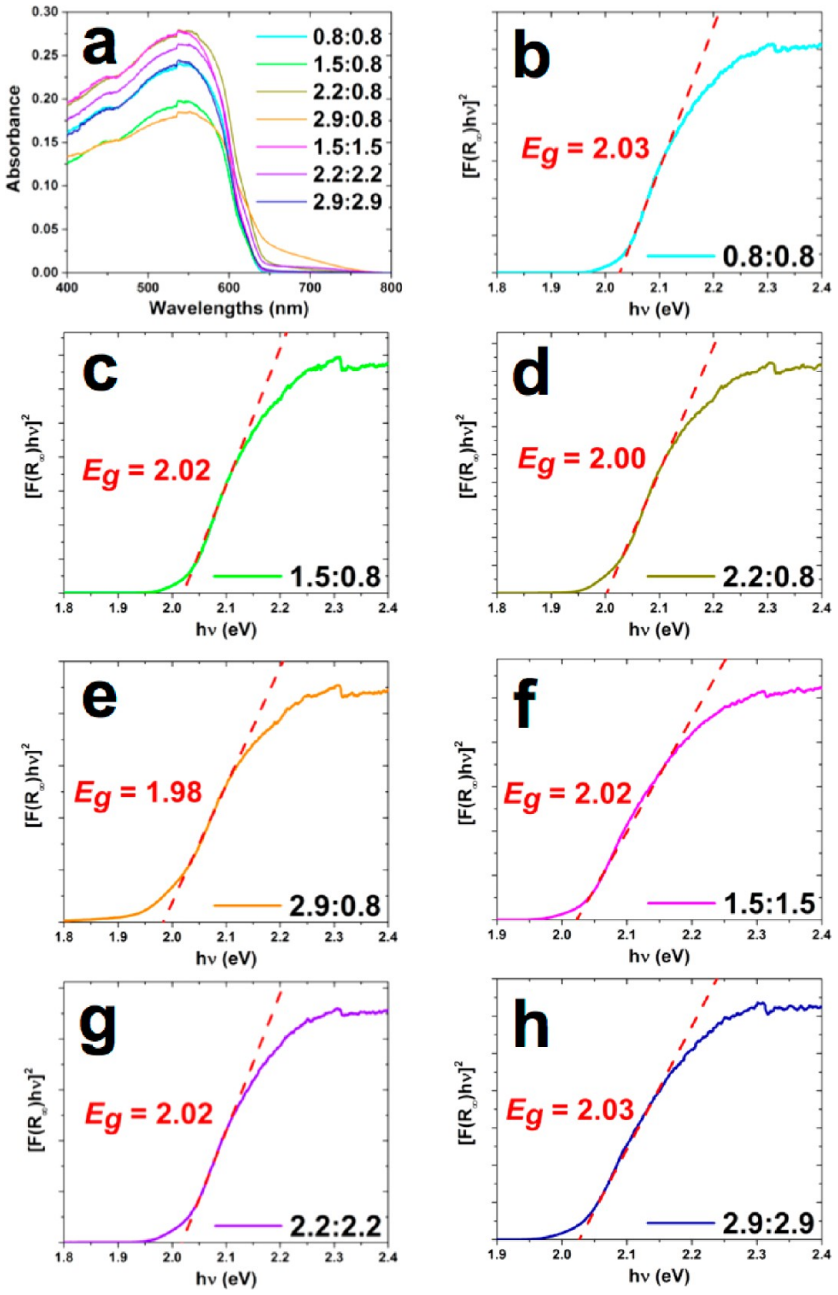

Figure 5. (a) UV-vis absorption spectra of the Cu_2O octahedral materials. (b–h) Tauc plots of the materials prepared at Cu^{2+}:glucose molar ratios of (b) 0.8:0.8, (c) 1.5:0.8, (d) 2.2:0.8, (e) 2.9:0.8, (f) 1.5:1.5, (g) 2.2:2.2, and (h) 2.9:2.9.

as observed via XPS. For instance, when the materials were fabricated at Cu^{2+}:glucose ratios of 1.5:0.8, 2.2:0.8, and 2.9:0.8, the band gap decreased to values of 2.02, 2.00, and 1.98 eV, respectively. This shift toward lower band gap values with increasing CuO amounts is not surprising, since CuO has a much smaller band gap (1.4 eV) than Cu_2O and, therefore, absorbs more visible light.[47] Furthermore, for the 1.5:1.5, 2.2:2.2, and 2.9:2.9 samples, the band gap ranged between 2.02 eV and 2.03 eV, which is consistent with the XPS compositional analysis, suggesting a higher fraction of Cu_2O in the materials.

Taken together, significant structural differences can be noted in these materials, based on the effect of the reductant. For this study, the major difference in the preparation process for the two different sets of materials was the amount of glucose introduced during the reaction: either a constant and lower glucose concentration (0.8 mmol) or a glucose concentration equal to the Cu^{2+} concentration. This generally resulted in greater amounts of CuO in the sample for those materials prepared at the highest Cu^{2+}:glucose ratios; however, these materials still maintained the octahedral structure. This suggests that the CTAB plays an important role in maintaining the shape, as supported by the control reactions studied with no surfactant. Interestingly, the particle size was dependent upon the Cu^{2+} concentration in the sample for both reaction conditions. This may occur based on manipulation of the nucleation and growth kinetics of the materials. In this regard, should similar numbers of nuclei be developed in each sample, regardless of the Cu^{2+} concentration, the overall particle edge length would increase, based on the amount of Cu^{2+} in the

DOI: 10.1021/acsami.5b04282
ACS Appl. Mater. Interfaces 2015, 7, 13238–13250

reaction, as observed herein. Should greater numbers of nuclei be developed as the Cu^{2+} concentration increases, additional sites for particle growth would be present in solution, resulting in smaller particles. Since this does not occur, this supports the formation of similar numbers of nuclei in each sample; however, additional studies are required to determine this fine level of detail.

Photocatalytic Reactivity. Once the materials were fully characterized, their photocatalytic reactivity was evaluated. For this, the photocatalytic degradation of aromatic organic compounds was examined using all of the prepared particles irradiated by a solar simulator. The reactivity of the materials was examined using two specific dyes—anionic methyl orange and cationic methylene blue—to ascertain the electrostatic effects on the material reactivity. In the first set of reactions, 10.0 mg of particles for each sample were mixed into an aqueous solution of the dye and allowed to equilibrate in darkness for 30 min, followed by light irradiation for 3.0 h. Figure 6a presents the UV-vis spectra of the degradation of methyl orange, using the 0.8:0.8 particles. In the spectrum prior to the reaction, a peak at 464 nm was observed, arising from the absorbance of the dye in the mixture. As the reaction ensues, the peak decreases, because of the photocatalytic degradation of the dye, until it is completely consumed. By monitoring the degradation of the dye over time, the kinetics of the reaction was determined and compared for each sample. Figure 6b presents the photodegradation analysis of methyl orange when a particle mass of 10.0 mg was used for each reaction. In this setup, the dye molecules were allowed to interact with the octahedra for 30 min prior to light irradiation; no changes in the concentration of the dye solution were observed when a catalyst mass of 10.0 mg was used for each reaction. Because of the conduction and valence band positions of the materials, it was anticipated that those structures with the greatest amount of Cu_2O would be the most reactive.[1,25,48] Interestingly, under these conditions, the Cu_2O structures prepared at a Cu^{2+}:glucose ratio of 1.5:0.8 were the most efficient for the degradation process. In this regard, 90% of the dye was degraded within 110 min, resulting in a pseudo-first-order rate constant (k_{mass}, which indicates that the kinetic analysis was completed using a Cu_2O mass of 10.0 mg) of $(2.01 \pm 0.17) \times 10^{-2}$ min^{-1}.[48,49] Such a result was quite interesting as this sample did not possess the greatest amount of Cu_2O in the material (64.0%), as compared to the octahedra prepared at a ratio of 0.8:0.8 (80.8%). For the latter sample, 170 min of irradiation was required to reach 90% degradation with a k_{mass} value of $(1.18 \pm 0.05) \times 10^{-2}$ min^{-1}. Further decreased rates of photodegradation were observed for the rest of the samples prepared (Table 1) when a catalyst mass of 10.0 mg was used for each reaction. Additional control studies were also conducted using commercially available bulk Cu_2O and CuO, both of which were inactive for the photocatalytic process. Generally, while the synthesized materials were photocatalytically reactive for the degradation of the anionic methyl orange dye, no evident trends, with respect to material composition, were observed, suggesting that additional structural properties of the oxides played a critical role in the overall reactivity.

While employing a constant catalyst mass is a standard process,[25,29,50] the actual catalytic surface area is likely to differ among the materials prepared at the different Cu^{2+}:glucose ratios. This is especially true due to changes in the material composition between the samples. To quantify such effects, BET analysis was conducted to determine the available catalytic surface area of the materials, which is summarized in Table 1. From this analysis, it is clear that drastically different surface areas are present for the materials ranging from 0.69 m^2/g to 12.93 m^2/g for the 0.8:0.8 to 2.9:0.8 samples, respectively. Note that the surface area observed by BET is larger than the calculated geometric surface area for nearly all of the Cu_2O octahedra, suggesting that the materials are porous (see Table S2 in the Supporting Information). This different surface area is likely to be quite important to the overall reactivity, in combination with the material composition; therefore, modified photocatalytic reactions were carried out where the total oxide

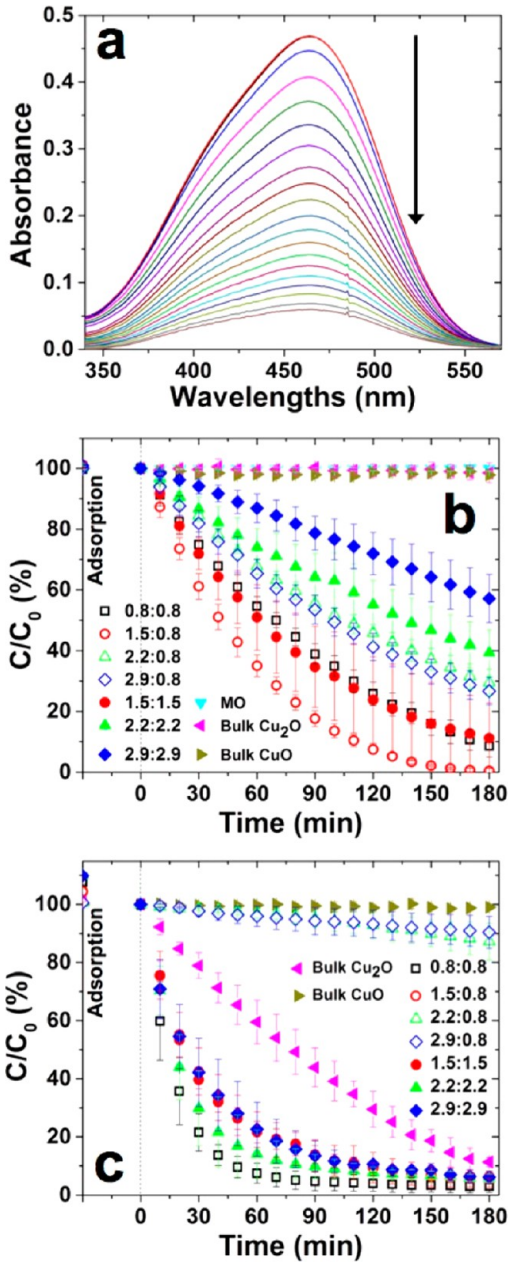

Figure 6. Photocatalytic degradation of methyl orange: (a) the degradation of the dye using the 0.8:0.8 sample at a loading of 10.0 mg in the reaction (spectra were collected every 10 min); (b, c) the overall analysis for the reaction for all of the particles studied when (b) a catalyst mass of 10.0 mg was used in the reaction and (c) a total oxide surface area of 0.065 m^2 was used in the reaction. Prior to light irradiation, the materials were allowed to interact with the dye molecules for 30 min in darkness.

DOI: 10.1021/acsami.5b04282
ACS Appl. Mater. Interfaces 2015, 7, 13238−13250

surface area (as determined by BET) was set constant to 0.065 m^2, and the catalyst mass employed in each reaction was varied. From this analysis, shown in Figure 6c, drastically different reactivities were observed for the materials for the photodegradation of methyl orange. Again, the materials were allowed to interact with the dye molecules for 30 min in darkness prior to light irradiation. Under constant-surface-area reaction conditions, dye adsorption was minimal (<10%), compared to the photodegradation activity, indicating that the removal of methyl orange was due to the photocatalytic activity of the Cu_2O. Almost complete degradation of the dye was achieved in 80 min when the 0.8:0.8 octahedra were employed as a catalyst. At this point in time, 95% of the dye was degraded, giving rise to a k_{SA} value (k_{SA}, which indicates that the kinetic analysis was for the 0.065 m^2 catalyst reactions) of $(5.16 \pm 0.66) \times 10^{-2}$ min^{-1}. When considering the other Cu^{2+}:glucose materials, a trend was clearly evident where the reaction rates were directly proportional to the composition of Cu_2O in the sample; when the amount of Cu_2O in the octahedral materials increased, the overall reaction rate also increased (see Table 1). This was anticipated based on the known conduction and valence band potentials of Cu_2O versus CuO, relative to the redox potentials for radical formation; although CuO has a much smaller band gap than Cu_2O and absorbs more visible light, the conduction band energy (E_{CB}) and the valence band energy (E_{VB}) of CuO are insufficient to catalyze the production of hydroxyl and superoxide radicals, which are primary initiators for the photocatalytic oxidation of aromatic organic compounds.[1,25,48] Although the presence of CuO is undesirable, CuO contamination is inevitable due to surface oxidation.[45] Therefore, it is essential to determine at what point the amount of CuO affects the photocatalytic activity. This is especially important for low-temperature synthetic routes in order to maximize Cu_2O amounts for increased reactivity. Based on the k_{SA} values, when the amount of surface Cu_2O in the octahedral materials is <50%, photocatalytic performance is significantly diminished.

When comparing the mass-constant and surface-area-constant studies, slight variations in the amount of dye adsorbed onto the oxide surface are noted. To investigate whether this process could reach equilibrium, the methyl orange dye was mixed with the 0.8:0.8 octahedra in darkness. Over time, aliquots were extracted, and the amount of dye adsorbed onto the particle surface was quantified for both the mass-constant and surface-area-constant conditions (see Figure S3 in the Supporting Information). Under the surface-area-constant conditions, minimal changes in the dye concentration in the reaction solution are evident, indicating that little dye adsorption occurred over the 6 h study. For the mass-constant conditions, however, a gradual decrease in the solution dye concentration was noted, which was consistent with removal of the dye from solution. In this regard, after 6 h, the dye concentration decreased by 71%. Interestingly, based on the reagent footprint, more dye would be adsorbed onto the oxide than what would be anticipated, based on the measured oxide surface area. This suggests that a slower, secondary dye degradation process is occurring; however, the rate for this process is substantially slow enough that it would not affect the photocatalytic process being studied, where 90% of the dye was degraded within <3 h, using these materials.

The effects of the surface area were also evident, wherein the catalysts with higher surface areas also had higher reactivities. This was apparent for the materials prepared at a Cu^{2+}:glucose ratio of 2.9:0.8. These samples had the lowest percentage of Cu_2O in the final structures (38.0%); therefore, they should have been the least reactive. When the reaction was carried out with a catalyst mass of 10.0 mg, they displayed a k_{mass} value of $(0.70 \pm 0.05) \times 10^{-2}$ min^{-1}, which was in the middle of the values observed. When considering the available surface area of these structures (12.93 m^2/g), this value represented the highest surface area per mass for all of the materials studied. As a result, the largest total surface area was presented for this sample when a constant catalyst mass of 10.0 mg was used in the reactions. When the reaction conditions were changed and the total surface area was set constant for each octahedra sample, the k_{SA} value significantly decreased to $(0.08 \pm 0.07) \times 10^{-2}$ min^{-1}, which was near the lowest value reported. One final point for the reactions employing a constant oxide surface area of 0.065 m^2, the k_{SA} reactivity became apparent for the bulk Cu_2O structures as these materials presented a very low specific surface area (0.40 m^2/g). As anticipated, no reactivity for the bulk CuO materials was observed, consistent with the band gap positioning. These results support the notion that the metal oxide surface participates in the reaction, either through electron transfer processes for radical formation or through dye adsorption.

Charged inorganic interfaces are typically developed when using oxide-based materials. Thus, the charge on the degrading substrate plays a role in the reactivity. The results above employed methyl orange, which is an anionic dye. The same reaction was studied using methylene blue, which is a cationic dye, and 10.0 mg of catalyst mass. Figure 7a presents the UV-vis spectra of the methylene blue degradation reaction using the

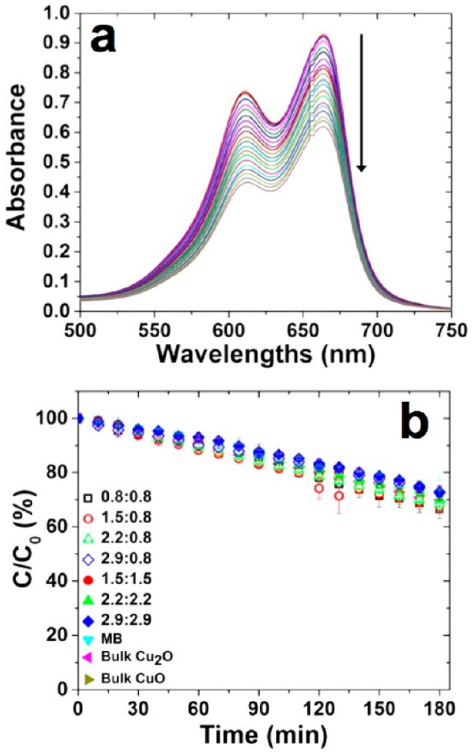

Figure 7. Photocatalytic degradation of methylene blue: (a) degradation of the dye using the 0.8:0.8 sample at a loading of 10.0 mg in the reaction (spectra were collected every 10 min); (b) overall analysis of the reaction for all of the particles studied when a catalyst mass of 10.0 mg was employed in the reaction.

DOI: 10.1021/acsami.5b04282
ACS Appl. Mater. Interfaces 2015, 7, 13238−13250

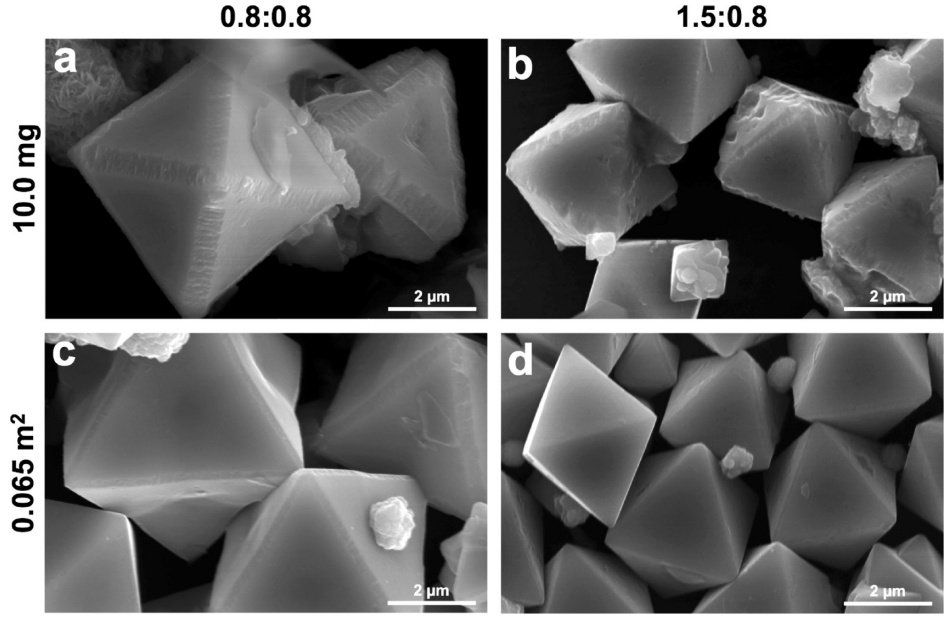

Figure 8. SEM images of the Cu_2O octahedra after the photodegradation of methyl orange. Panels a and c present the 0.8:0.8 materials when (a) a catalyst mass of 10.0 mg was used in the reaction and (c) a total surface area of 0.065 m^2 was used in the reaction. Panels b and d present the 1.5:0.8 materials when (b) a catalyst mass of 10.0 mg was used in the reaction and (d) a total surface area of 0.065 m^2 was used in the reaction. Scale bars = 2 μm.

0.8:0.8 particles. A peak at 664 nm was observed in the spectrum prior to the reaction, arising from the absorbance of the dye. When any of the octahedral materials were employed as the catalyst, no enhanced methylene blue degradation was noted, compared to the catalyst-free system, suggesting no catalytic effect of the particles toward methylene blue (Figure 7b). This behavior is consistent with previous observations for Cu_2O octahedra and hexapods bound by {111} facets that display positively charged Cu^+ atoms, suggesting that the surface of the octahedra is positively charged to repel the cationic dye.[13,51] This would explain the lack of reactivity for the degradation of the cationic methylene blue dye, in contrast to the rapid degradation reactivity for the anionic methyl orange dye that is electrostatically attracted to the positively charged oxide. This also supports the hypothesis that some type of interaction between the substrate and surface is required for photocatalytic reactivity; should the dye not interact with the oxide surface, no charge effects should be evident for the different reactions.

Taken together, these catalytic results suggest that both the composition of the materials, which affects the photogeneration of electron/hole pairs, and the available oxide surface area play a role in the overall reaction. Generally, for all of the reactions, increased reactivity is noted from materials with greater Cu_2O compositions. This is specifically noted in the reactions where the total surface area was set to 0.065 m^2, but is also generally evident in the reactions where a 10.0 mg catalyst mass was employed. When considering systems with similar Cu_2O compositions, those materials with greater surface areas were generally more reactive. This suggests that the substrate must interact with the oxide surface, in combination with the reactive oxygen species, to drive the dye degradation process. As such, both electron/hole pair formation and available surface area played an important role in the overall reactivity.

For Cu_2O, a key issue is photostability, since photocorrosion leads to the reduction of its photocatalytic activity.[52] Therefore, the photostability of the 0.8:0.8 and 1.5:0.8 Cu_2O octahedra particles was investigated; these materials were selected because they exhibited the highest k_{SA} and k_{mass} values, respectively. Figure 8 presents SEM images of the particles after the photocatalytic degradation of methyl orange under both 10.0 mg mass and 0.065 m^2 surface area reaction conditions. Additional SEM images of all the materials presented for the photostability analysis can be found in the Supporting Information (Figures S7 and S8). Imaging of the octahedra post-photodegradation when a particle mass of 10.0 mg was used for each reaction (Figures 8a and 8b) shows that the particles undergo surface etching at the edges and vertices while retaining their octahedral structure. Similar surface reconstructions were observed when the total surface area was set constant in the reaction (Figures 8c and 8d); however, the etching is not as drastic, since a greater mass of material was employed to reach a surface area of 0.065 m^2. XRD was further used to study each post-reaction material (see Figure S4 in the Supporting Information). The XRD patterns show that the composition of the structures remained unchanged, with no reflections arising from CuO or Cu under both constant-mass or constant-surface-area conditions.

To ensure that the surface etching is due to photocatalysis, a series of control studies were conducted. SEM analysis of the 0.8:0.8 materials after a 6 h dye adsorption equilibration period in darkness under both constant-mass and constant-surface-area conditions (see Figure S5 in the Supporting Information) showed that no surface reconstruction occurred. In a second control, the 0.8:0.8 particles under both constant-mass and constant-surface-area conditions were photoirradiated in water for 3 h in the absence of dye. Here, surface etching on the edges and vertices of the octahedra was again observed (see Figure S6 in the Supporting Information); however, pitting of the {111} facets became more pronounced. This suggests that radical formation is likely occurring at the edges, where the pitting

DOI: 10.1021/acsami.5b04282
ACS Appl. Mater. Interfaces 2015, 7, 13238−13250

effect indicates that the particles are being photocorroded when no dye molecules are present.[53,54]

Taken together, these post-reaction analyses provide important information concerning the catalytic activity of the Cu_2O materials. In the reaction system with the dye, etching of the octahedra edges with minimal surface pitting is evident. This suggests that electron migration and the formation of the reactive oxygen species preferentially occurs at the particle edges and vertices, giving rise to the etching effect. Such a mechanistic hypothesis is supported by both the XRD and SEM controls. In this regard, the XRD analysis confirmed that no significant compositional change in the materials was evident, with Cu_2O forming the bulk of the structure. Adsorption of the dye to the oxide surface also did not result in changes to the octahedral shape; however, irradiation of the materials in the absence of the dye did give rise to edge etching and pitting of the {111} facets. Without any dye present in solution, the Cu_2O materials undergo photocorrosion. Based on the electrostatic results observed for the cationic and anionic dyes, it is likely that the methyl orange is adsorbed onto the Cu_2O facets; however, additional characterization would be required to confirm this hypothesis. Nevertheless, these post-reaction analyses indicate that the redox reactions for reactive oxygen species preferentially occur at the particle edges and vertices to drive dye degradation.

CONCLUSION

In summary, we have generated size-controlled Cu_2O octahedral microcrystals via a facile synthetic approach using aqueous solutions at low temperatures. It has been demonstrated that the size of the octahedra can be tuned by changing the concentrations of the reagents, and that higher amounts of reductant result in materials with a greater Cu^+ content. In addition, the octahedral shape of the structures was maintained, regardless of material composition, but was dependent on the CTAB in the mixture. Furthermore, the as-synthesized octahedra were highly effective photocatalysts for the decomposition of the anionic methyl orange dye, but demonstrated minimal photocatalytic activity for cationic methylene blue. The results indicate that three specific considerations controlled the overall reaction rate: the charge of the inorganic interface, the composition of the materials, and the surface area of the catalytic structures. Post-photodegradation analysis showed that (i) the Cu_2O octahedra were stable and (ii) particle surface etching had occurred, specifically on the edges of the particles, suggesting that the redox reactions preferentially occurred at these regions. These four characteristics worked in concert to mediate the overall reactivity, which could be selectively tuned by the synthetic pathway to achieve different sizes and compositions of these materials, providing enhanced control over the catalytic properties. Such results could be important in metal oxide catalyst design, where the size and composition of the structure are key elements in obtaining sustainable and efficient catalytic functionality.

ASSOCIATED CONTENT

Supporting Information

Size distribution histograms, shape-control analyses, calculated geometric surface areas, and additional SEM images of the materials post-photodegradation. The Supporting Information is available free of charge on the ACS Publications website at DOI: 10.1021/acsami.5b04282.

AUTHOR INFORMATION

Corresponding Author

*Tel.: (305) 284-9351. E-mail: knecht@miami.edu.

Notes

The authors declare no competing financial interest.

ACKNOWLEDGMENTS

We would like to thank the University of Miami for financial support of this research. M.A.N. acknowledges fellowships from the Science Made Sensible program and the Howard Hughes Medical Institute. This research used resources of the Advanced Photon Source, a U.S. Department of Energy (DOE) Office of Science User Facility operated for the DOE Office of Science by Argonne National Laboratory, under Contract No. DE-AC02-06CH11357.

REFERENCES

(1) Teoh, W. Y.; Scott, J. A.; Amal, R. Progress in Heterogeneous Photocatalysis: From Classical Radical Chemistry to Engineering Nanomaterials and Solar Reactors. *J. Phys. Chem. Lett.* **2012**, *3*, 629−639.

(2) Joshi, U. A.; Palasyuk, A.; Arney, D.; Maggard, P. A. Semiconducting Oxides to Facilitate the Conversion of Solar Energy to Chemical Fuels. *J. Phys. Chem. Lett.* **2010**, *1*, 2719−2726.

(3) Zahran, E. M.; Bedford, N. M.; Nguyen, M. A.; Chang, Y.-J.; Guiton, B. S.; Naik, R. R.; Bachas, L. G.; Knecht, M. R. Light-Activated Tandem Catalysis Driven by Multicomponent Nanomaterials. *J. Am. Chem. Soc.* **2014**, *136*, 32−35.

(4) Haider, Z.; Kang, Y. S. Facile Preparation of Hierarchical TiO_2 Nano Structures: Growth Mechanism and Enhanced Photocatalytic H_2 Production from Water Splitting Using Methanol as a Sacrificial Reagent. *ACS Appl. Mater. Interfaces* **2014**, *6*, 10342−10352.

(5) Janet, C. M.; Navaladian, S.; Viswanathan, B.; Varadarajan, T. K.; Viswanath, R. P. Heterogeneous Wet Chemical Synthesis of Superlattice-Type Hierarchical ZnO Architectures for Concurrent H_2 Production and N_2 Reduction. *J. Phys. Chem. C* **2010**, *114*, 2622−2632.

(6) Xu, H.; Ouyang, S.; Li, P.; Kako, T.; Ye, J. High-Active Anatase TiO_2 Nanosheets Exposed with 95% {100} Facets Toward Efficient H_2 Evolution and CO_2 Photoreduction. *ACS Appl. Mater. Interfaces* **2013**, *5*, 1348−1354.

(7) Liu, L.; Zhao, H.; Andino, J. M.; Li, Y. Photocatalytic CO_2 Reduction with H_2O on TiO_2 Nanocrystals: Comparison of Anatase, Rutile, and Brookite Polymorphs and Exploration of Surface Chemistry. *ACS Catal.* **2012**, *2*, 1817−1828.

(8) Kondalkar, V. V.; Mali, S. S.; Mane, R. M.; Dandge, P. B.; Choudhury, S.; Hong, C. K.; Patil, P. S.; Patil, S. R.; Kim, J. H.; Bhosale, P. N. Photoelectrocatalysis of Cefotaxime Using Nanostructured TiO_2 Photoanode: Identification of the Degradation Products and Determination of the Toxicity Level. *Ind. Eng. Chem. Res.* **2014**, *53*, 18152−18162.

(9) Li, J.; Lv, S.; Liu, Y.; Bai, J.; Zhou, B.; Hu, X. Photoeletrocatalytic Activity of an *n*-ZnO/*p*-Cu_2O/*n*-TNA Ternary Heterojunction Electrode for Tetracycline Degradation. *J. Hazard. Mater.* **2013**, *262*, 482−488.

(10) Sayigh, A. A. M. *Solar Energy Engineering*; Academic Press: New York, 1977.

(11) Banerjee, S.; Pillai, S. C.; Falaras, P.; O'Shea, K. E.; Byrne, J. A.; Dionysiou, D. D. New Insights into the Mechanism of Visible Light Photocatalysis. *J. Phys. Chem. Lett.* **2014**, *5*, 2543−2554.

(12) Wang, J.; Wang, Z.; Huang, B.; Ma, Y.; Liu, Y.; Qin, X.; Zhang, X.; Dai, Y. Oxygen Vacancy Induced Band-Gap Narrowing and Enhanced Visible Light Photocatalytic Activity of ZnO. *ACS Appl. Mater. Interfaces* **2012**, *4*, 4024−4030.

(13) Ho, J.-Y.; Huang, M. H. Synthesis of Submicrometer-Sized Cu_2O Crystals with Morphological Evolution from Cubic to Hexapod

DOI: 10.1021/acsami.5b04282
ACS Appl. Mater. Interfaces 2015, 7, 13238−13250

Structures and Their Comparative Photocatalytic Activity. *J. Phys. Chem. C* **2009**, *113*, 14159−14164.
(14) Zhao, Y.-F.; Yang, Z.-Y.; Zhang, Y.-X.; Jing, L.; Guo, X.; Ke, Z.; Hu, P.; Wang, G.; Yan, Y.-M.; Sun, K.-N. Cu_2O Decorated with Cocatalyst MoS_2 for Solar Hydrogen Production with Enhanced Efficiency under Visible Light. *J. Phys. Chem. C* **2014**, *118*, 14238−14245.
(15) Zhang, L.; Jing, D.; Guo, L.; Yao, X. *In Situ* Photochemical Synthesis of Zn-Doped Cu_2O Hollow Microcubes for High Efficient Photocatalytic H_2 Production. *ACS Sustainable Chem. Eng.* **2014**, *2*, 1446−1452.
(16) Jeong, S. S.; Mittiga, A.; Salza, E.; Masci, A.; Passerini, S. Electrodeposited ZnO/Cu_2O Heterojunction Solar Cells. *Electrochim. Acta* **2008**, *53*, 2226−2231.
(17) Morales, J.; Sánchez, L.; Bijani, S.; Martínez, L.; Gabás, M.; Ramos-Barrado, J. R. Electrodeposition of Cu_2O: An Excellent Method for Obtaining Films of Controlled Morphology and Good Performance in Li-Ion Batteries. *Electrochem. Solid-State Lett.* **2005**, *8*, A159−A162.
(18) Poizot, P.; Laruelle, S.; Grugeon, S.; Dupont, L.; Tarascon, J.-M. Nano-sized Transition-Metal Oxides as Negative-Electrode Materials for Lithium-Ion Batteries. *Nature* **2000**, *407*, 496−499.
(19) Xu, C.; Cao, L.; Su, G.; Liu, W.; Liu, H.; Yu, Y.; Qu, X. Preparation of ZnO/Cu_2O Compound Photocatalyst and Application in Treating Organic Dyes. *J. Hazard. Mater.* **2010**, *176*, 807−813.
(20) Li, S.-K.; Huang, F.-Z.; Wang, Y.; Shen, Y.-H.; Qiu, L.-G.; Xie, A.-J.; Xu, S.-J. Magnetic Fe_3O_4@C@Cu_2O Composites with Bean-like Core/Shell Nanostructures: Synthesis, Properties and Application in Recyclable Photocatalytic Degradation of Dye Pollutants. *J. Mater. Chem.* **2011**, *21*, 7459−7466.
(21) Jing, H.-Y.; Wen, T.; Fan, C.-M.; Gao, G.-Q.; Zhong, S.-L.; Xu, A.-W. Efficient Adsorption/Photodegradation of Organic Pollutants from Aqueous Systems Using Cu_2O Nanocrystals as a Novel Integrated Photocatalytic Adsorbent. *J. Mater. Chem. A* **2014**, *2*, 14563−14570.
(22) Xiong, J.; Li, Z.; Chen, J.; Zhang, S.; Wang, L.; Dou, S. Facile Synthesis of Highly Efficient One-Dimensional Plasmonic Photocatalysts through Ag@Cu_2O Core−Shell Heteronanowires. *ACS Appl. Mater. Interfaces* **2014**, *6*, 15716−15725.
(23) Yu, L.; Xi, J.; Li, M.-D.; Chan, H. T.; Su, T.; Phillips, D. L.; Chan, W. K. The Degradation Mechanism of Methyl Orange under Photo-catalysis of TiO_2. *Phys. Chem. Chem. Phys.* **2012**, *14*, 3589−3595.
(24) Padmaja, S.; Madison, S. A. Hydroxyl Radical-Induced Oxidation of Azo Dyes: A Pulse Radiolysis Study. *J. Phys. Org. Chem.* **1999**, *12*, 221−226.
(25) Cao, J.; Luo, B.; Lin, H.; Xu, B.; Chen, S. Visible Light Photocatalytic Activity Enhancement and Mechanism of AgBr/Ag_3PO_4 Hybrids for Degradation of Methyl Orange. *J. Hazard. Mater.* **2012**, *217*−*218*, 107−115.
(26) Gou, L.; Murphy, C. J. Controlling the Size of Cu_2O Nanocubes from 200 to 25 nm. *J. Mater. Chem.* **2004**, *14*, 735−738.
(27) Sui, Y.; Fu, W.; Yang, H.; Zeng, Y.; Zhang, Y.; Zhao, Q.; Li, Y.; Zhou, X.; Leng, Y.; Li, M.; Zou, G. Low Temperature Synthesis of Cu_2O Crystals: Shape Evolution and Growth Mechanism. *Cryst. Growth Des.* **2010**, *10*, 99−108.
(28) Xu, H.; Wang, W.; Zhu, W. Shape Evolution and Size-Controllable Synthesis of Cu_2O Octahedra and Their Morphology-Dependent Photocatalytic Properties. *J. Phys. Chem. B* **2006**, *110*, 13829−13834.
(29) Huang, W.-C.; Lyu, L.-M.; Yang, Y.-C.; Huang, M. H. Synthesis of Cu_2O Nanocrystals from Cubic to Rhombic Dodecahedral Structures and Their Comparative Photocatalytic Activity. *J. Am. Chem. Soc.* **2011**, *134*, 1261−1267.
(30) Xu, Y.; Wang, H.; Yu, Y.; Tian, L.; Zhao, W.; Zhang, B. Cu_2O Nanocrystals: Surfactant-Free Room-Temperature Morphology-Modulated Synthesis and Shape-Dependent Heterogeneous Organic Catalytic Activities. *J. Phys. Chem. C* **2011**, *115*, 15288−15296.
(31) Liang, Y.; Shang, L.; Bian, T.; Zhou, C.; Zhang, D.; Yu, H.; Xu, H.; Shi, Z.; Zhang, T.; Wu, L.-Z.; Tung, C.-H. Shape-Controlled Synthesis of Polyhedral 50-Facet Cu_2O Microcrystals with High-Index Facets. *CrystEngComm* **2012**, *14*, 4431−4436.
(32) Cao, Y.; Fan, J.; Bai, L.; Yuan, F.; Chen, Y. Morphology Evolution of Cu_2O from Octahedra to Hollow Structures. *Cryst. Growth Des.* **2010**, *10*, 232−236.
(33) Yang, H.; Liu, Z.-H. Facile Synthesis, Shape Evolution, and Photocatalytic Activity of Truncated Cuprous Oxide Octahedron Microcrystals with Hollows. *Cryst. Growth Des.* **2010**, *10*, 2064−2067.
(34) Cao, M.; Hu, C.; Wang, Y.; Guo, Y.; Guo, C.; Wang, E. A Controllable Synthetic Route to Cu, Cu_2O, and CuO Nanotubes and Nanorods. *Chem. Commun.* **2003**, 1884−1885.
(35) Hammersley, A. FIT2D. Available via the Internet at: http://www.esrf.eu/computing/scientific/FIT2D/ (accessed May 6, 2015).
(36) Zhu, C.; Guo, S.; Fang, Y.; Dong, S. Reducing Sugar: New Functional Molecules for the Green Synthesis of Graphene Nanosheets. *ACS Nano* **2010**, *4*, 2429−2437.
(37) Hacialioglu, S.; Meng, F.; Jin, S. Facile and Mild Solution Synthesis of Cu_2O Nanowires and Nanotubes Driven by Screw Dislocations. *Chem. Commun.* **2012**, *48*, 1174−1176.
(38) Liu, H.; Miao, W.; Yang, S.; Zhang, Z.; Chen, J. Controlled Synthesis of Different Shapes of Cu_2O via γ-Irradiation. *Cryst. Growth Des.* **2009**, *9*, 1733−1740.
(39) Sun, S.; Zhou, F.; Wang, L.; Song, X.; Yang, Z. Template-Free Synthesis of Well-Defined Truncated Edge Polyhedral Cu_2O Architectures. *Cryst. Growth Des.* **2010**, *10*, 541−547.
(40) Database of Raman Spectra, X-ray Diffraction and Chemistry of Minerals. Available via the Internet at: http://rruff.info/ (accessed May 6, 2015).
(41) Deroubaix, G.; Marcus, P. X-ray Photoelectron Spectroscopy Analysis of Copper and Zinc Oxides and Sulphides. *Surf. Interface Anal.* **1992**, *18*, 39−46.
(42) Chusuei, C. C.; Brookshier, M. A.; Goodman, D. W. Correlation of Relative X-ray Photoelectron Spectroscopy Shake-up Intensity with CuO Particle Size. *Langmuir* **1999**, *15*, 2806−2808.
(43) An, X.; Li, K.; Tang, J. Cu_2O/Reduced Graphene Oxide Composites for the Photocatalytic Conversion of CO_2. *ChemSusChem* **2014**, *7*, 1086−1093.
(44) Liu, H.; Wang, J.; Fan, X. M.; Zhang, F. Z.; Liu, H. R.; Dai, J.; Xiang, F. M. Synthesis of Cu_2O/T-ZnO_W Nanocompound and Characterization of Its Photocatalytic Activity and Stability Property under UV Irradiation. *Mater. Sci. Eng., B* **2013**, *178*, 158−166.
(45) Liu, P.; Li, Z.; Cai, W.; Fang, M.; Luo, X. Fabrication of Cuprous Oxide Nanoparticles by Laser Ablation in PVP Aqueous Solution. *RSC Adv.* **2011**, *1*, 847−851.
(46) Morales, A. E.; Mora, E. S.; Pal, U. Use of Diffuse Reflectance Spectroscopy for Optical Characterization of Unsupported Nanostructures. *Rev. Mex. Fis. S* **2007**, *53*, 18−22.
(47) Ghijsen, J.; Tjeng, L. H.; van Elp, J.; Eskes, H.; Westerink, J.; Sawatzky, G. A.; Czyzyk, M. T. Electronic Structure of Cu_2O and CuO. *Phys. Rev. B* **1988**, *38*, 11322−11330.
(48) Chen, H.; Leng, W.; Xu, Y. Enhanced Visible-Light Photoactivity of $CuWO_4$ through a Surface-Deposited CuO. *J. Phys. Chem. C* **2014**, *118*, 9982−9989.
(49) Andronic, L.; Duta, A. The Influence of TiO_2 Powder and Film on the Photodegradation of Methyl Orange. *Mater. Chem. Phys.* **2008**, *112*, 1078−1082.
(50) Liu, L.; Yang, W.; Li, Q.; Gao, S.; Shang, J. K. Synthesis of Cu_2O Nanospheres Decorated with TiO_2 Nanoislands, Their Enhanced Photoactivity and Stability under Visible Light Illumination, and Their Post-illumination Catalytic Memory. *ACS Appl. Mater. Interfaces* **2014**, *6*, 5629−5639.
(51) Yang, S.; Zhang, S.; Wang, H.; Yu, H.; Fang, Y.; Peng, F. Facile Synthesis of Self-Assembled Mesoporous CuO Nanospheres and Hollow Cu_2O Microspheres with Excellent Adsorption Performance. *RSC Adv.* **2014**, *4*, 43024−43028.
(52) Huang, L.; Peng, F.; Yu, H.; Wang, H. Preparation of Cuprous Oxides with Different Sizes and Their Behaviors of Adsorption,

DOI: 10.1021/acsami.5b04282
ACS Appl. Mater. Interfaces 2015, 7, 13238−13250

Visible-Light Driven Photocatalysis and Photocorrosion. *Solid State Sci.* **2009**, *11*, 129−138.
(53) Pan, L.; Zou, J.-J.; Zhang, T.; Wang, S.; Li, Z.; Wang, L.; Zhang, X. Cu_2O Film via Hydrothermal Redox Approach: Morphology and Photocatalytic Performance. *J. Phys. Chem. C* **2014**, *118*, 16335−16343.
(54) Zheng, Z.; Huang, B.; Wang, Z.; Guo, M.; Qin, X.; Zhang, X.; Wang, P.; Dai, Y. Crystal Faces of Cu_2O and Their Stabilities in Photocatalytic Reactions. *J. Phys. Chem. C* **2009**, *113*, 14448−14453.

DOI: 10.1021/acsami.5b04282
ACS Appl. Mater. Interfaces 2015, 7, 13238−13250